A SVM-3D Based Sensorless Speed Control of a Fault-Tolerant PMSMs Fed by 27 Level Inverter

Kamel Saleh[a]* and M. Sumner[b]

[a]*Electrical Engineering Dept, An-Najah National University, Nablus, Palestine;*

[b]*Electrical Engineering Dept, Nottingham University, Nottingham, UK*

*kamel.saleh@najah.edu. mark.sumner@nottingham.ac.uk

A SVM-3D Based Sensorless Speed Control of a Fault-Tolerant PMSMs Fed by 27 Level Inverter

Abstract: This paper deals with a sensorless control of a permanent magnet synchronous motor post an open-circuit fault condition to achieve a maximum reliability of the whole drive system. To achieve that, a 4-leg 27-level Cascaded H-Bridge inverter modulated through a 3-Dimension Space Vector Modulation technique (3D-SVM) is used to make the hole drive system fault-tolerant. Besides that, an algorithm to track the saturation saliency position post an open-circuit fault is used. This algorithm is based on measuring the transient current response of the motor line currents due to the IGBTs switching actions. Then according to the operating condition (healthy or post an open-circuit fault) the saliency position signals are constructed from the dynamic current responses. Simulation results are provided to demonstrate the effectiveness of the saliency tracking technique under healthy and post an open-circuit fault condition. Moreover, the results will verify the maximum reliability for the whole drive system that is achieved in this work through a continuous operation of the drive system post an-open circuit fault condition and under sensorless speed control.

Keywords: word; fault-tolerant multi-level inverter, sensorless, single-phase open circuit, 3D SVM

1. INTRODUCTION

Multilevel inverters are a very attractive solution in high power applications (Ying & Gan, 2012), medium voltage(Marzoughi ,Burgos, Boroyevich, & Xue, 2014) including high- speed railways (Qashqai, Sheikholeslami, Vahedi, & Al-Haddad, 2015), renewable energy sources (Yu, Konstantinou, Hredzak, & Agelidis, 2016). This is due to their capability to handle high voltage and at the same time produce an output voltage near sinusoidal (low Total Harmonic Distortion THD) (Bhagwat, & Stefanovic, 1983; Lai, & Peng, 1996; Okazaki , Matsui, Moses, Muhoro, Hagiwara , & Akagi, 2016). The multi-level inverter has many topologies such as the cascaded H-bridge (CHB), neutral point clamped (NPC), and flying capacitor inverters (Nabae, Takahashi, & Akagi, 1981; P.

Hammond,1997; Meynard, Foch, Thomas, Courault, Jakob, & Nahrstaed, 2002). The advantages coming from the elimination of cabling and mechanical sensors in terms of increasing the reliability and reducing the cost has directed the researchers towards sensorless control of two-level and multi-level inverter drive system sensorless techniques. Sensorless control techniques of multi-level inverter drive are similar to those used in two-level inverter drive and can be divided into two main groups. The first group is called model-based group (Adiuku, Beig, & Kanukollu, 2015; Wang, & Lu 2010; Kim, Chan, & Kwak2017; Kant, & Singh 2018) , and these techniques fails at low and zero speeds. The second group is known as signal injection group dealing with spatial saliencies (Scelba, Scarcella, Foti, De Caro, & Testa, 2017; Saleh, Asher, Sumner, Tomasini, & Qiang, 2009; Saleh, Sumner, 2016). Spatial saliency tracking methods inject high frequency current or voltage components in addition to the fundamental one. A suitable demodulation of the stator currents and/or voltages allows to extract useful information about the position of the rotor.

In certain applications like electric vehicles, aerospace systems, military, hospitals, the shutdown of the electrical systems due to any fault in the inverter may result in a potential risk to human beings and immeasurable economic losses (Welchko, Lipo , Jahns, & Schulz, 2004; Haimin, Duarte, & Hendrix, 2008). Hence, these applications require a reliable inverter that enables the continuous operation of the system post the fault. Therefore, discussion of fault-tolerant inverters and enhanced system reliability attracts much attention among researchers.

Fault-tolerant inverters are reported in many papers in literature. These fault-tolerant inverters make use of the hardware redundancy to achieve post-fault operation (Zhang, Xu, Enjeti, Li, Hawke, & Krishnamoorthy, 2014). Based on the hardware redundancy, the fault-tolerant inverters can be classified into three groups. The first group

deals with switch fault to achieve post-fault operation using different techniques like inherently redundant witching states (Lezana, Pou, Meynard, Rodriguez, Ceballos, & Richardeau, 2010), DC-bus midpoint connection(Campos-Delgado, Espinoza-Trejo, & Palacios, 2008) and redundant parallel or series switches installation (Rodriguez, Claudio, Theilliol, Vela, & Hernandez, 2008). The second group deals with leg fault to achieve post-fault operation by adding redundant legs in parallel or series connection to the main legs (Jen-Ren & Lipo, 1993; Mohammad pour, Sadeghi, & Parsa, 2014). finally, post fault operation can be achieved in multi-level inverter using three scenarios including neutral-shift, DC-bus voltage reconfiguration, and redundant modules installation are employed (Yi, Hongge , & Bin, 2008; Lezana, & Ortiz, 2009; Correa, Pacas, & Rodriguez, 2006). Sensorless control of motor drives under open circuits phase faults are proposed (Saleh, & Sumner,2016) using a four-leg two-level (PMSM) drive and in (Saleh, & Sumner,2018) using four-leg multi-level (PMSM) drive. A special fault-tolerant control technique was used in cases of an open circuit fault to keep the performance of the drive from degradation.

This paper is introducing a novel method to achieve sensorless speed control of a permanent magnet synchronous motor post an open-circuit fault condition to achieve a maximum reliability of the whole drive system. The reliability of the system is maximized by using two techniques. The first one is the use of a 4-leg 27-level inverter based on 3D SVPWM modulation technique to maintain continuous system operation post of an open circuit fault. The second technique is to introduce algorithm to track the saturation saliency of PMSM post the open circuit fault. These two procedures help to meet the safety procedure for the whole system and increase the reliability of the system.

2. Four-Leg Multi-Level Drive Topology

Figure 1 shows the proposed four-leg muli-level inverter drive topology. An overview of each part of this topology is illustrated below.-

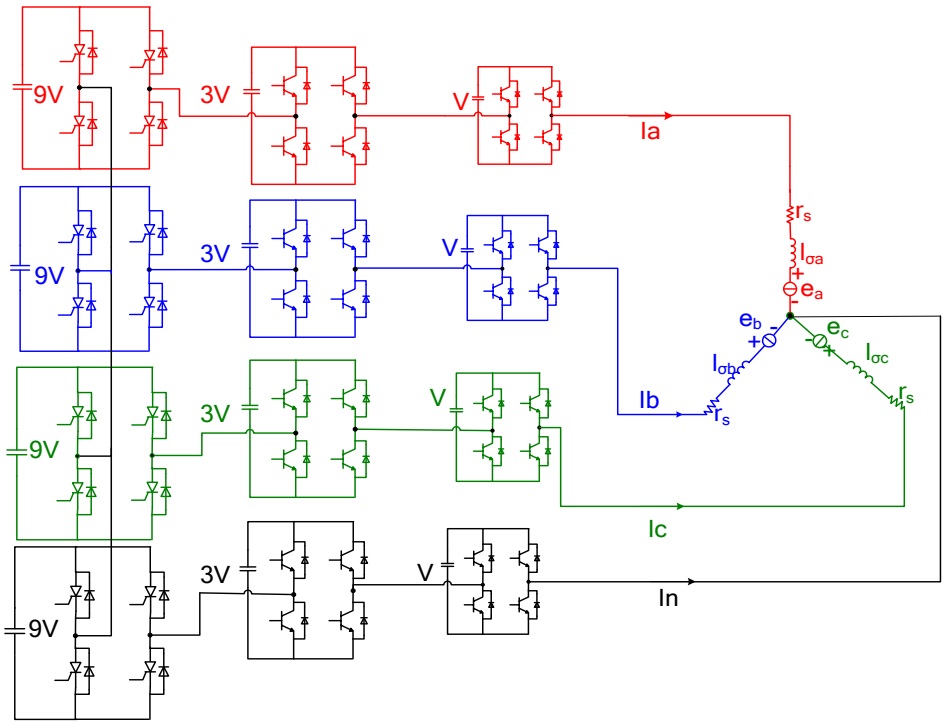

Figure 1. 4-leg 27-level PMSM drive

2.1 Three phase PMSM model

The three phase PMSM model is given in equations (1-5). In this model the saturation saliency is inherited in the self and leakage inductances equations. Moreover, this model can give trusted result in healthy operating conditions and in the cases of some fault conditions like open-circuit fault.

$$\begin{bmatrix} v_a \\ v_b \\ v_c \end{bmatrix} = r_s * \begin{bmatrix} i_a \\ i_b \\ i_c \end{bmatrix} + \begin{bmatrix} d\emptyset_a/dt \\ d\emptyset_b/dt \\ d\emptyset_c/dt \end{bmatrix} \quad (1)$$

$$\begin{bmatrix} \emptyset_a \\ \emptyset_b \\ \emptyset_c \end{bmatrix} = \begin{bmatrix} L_{aa} L_{ab} L_{ac} L_{ad} L_{ae} \\ L_{ab} L_{bb} L_{bc} L_{bd} L_{be} \\ L_{ac} L_{bc} L_{cc} L_{cd} L_{ce} \end{bmatrix} \begin{bmatrix} i_a \\ i_b \\ i_c \end{bmatrix} + \begin{bmatrix} \varphi_{ma} \\ \varphi_{mb} \\ \varphi_{mc} \end{bmatrix} \quad (2)$$

Where $v_{a,b,c}$ are the external voltages applied to the motor, r_s is the equivalent resistance

of the stator winding, $i_{a,b,c}$ are the stator phase currents , $\emptyset_{a,b,c}$ are the total fluxes linking stator windings,L_{aa}, L_{bb} and L_{cc} are the total-inductances of the stator windings and L_{ab}, L_{ac} and L_{bc} are the mutual inductances of the stator windings. $\varphi_{ma,b,c}$ is the permanent magnet fluxes linking the stator windings.

The inductances in the stator windings are functions of rotor angle, defined by :-

$$\begin{bmatrix} L_{aa} \\ L_{bb} \\ L_{cc} \end{bmatrix} = \begin{bmatrix} L_{so} + L_{sl} \\ L_{so} + L_{sl} \\ L_{so} + L_{sl} \end{bmatrix} + L_x * \begin{bmatrix} cos(2\theta) \\ cos(2\theta - 120) \\ cos(2\theta - 240 \end{bmatrix} (3)$$

$$\begin{bmatrix} L_{ab} \\ L_{ac} \\ L_{bc} \end{bmatrix} = L_{so} * \begin{bmatrix} \cos(120) \\ \cos(240) \\ \cos(120) \end{bmatrix} + L_x * \begin{bmatrix} \cos(2\theta - 120) \\ \cos(2\theta - 120) \\ \cos(2\theta - 120) \end{bmatrix} (4)$$

where: L_{sl}, L_x are the stator self and fluctuating inductances per phase respectively . $L_{so}$is the stator mutual inductance. It is worth to say here that equation(4) is inherently including the saturation saliency effect which appears in the term (2θ). Finally, the permanent magnet fluxes linking the stator winding are:-

$$\begin{bmatrix} \varphi_{ma} \\ \varphi_{mb} \\ \varphi_{mc} \end{bmatrix} = \Lambda_m * \begin{bmatrix} cos(\theta) \\ cos(\theta - 120) \\ cos(\theta - 240) \end{bmatrix} (5)$$

where Λ_m is the peak flux linkage due to permanent magnet.

2.2 27-level Inverter

Asymmetric cascaded multi-level inverter is used in this research. Each leg of the inverter consists of three H-bridges connected in series and supplied by three independent DC sources a scaled in the power of three as shown in figure 2. This configuration of the multi-level inverter helps to generate 27-level at the output of the inverter instead of generating 7 levels when using symmetric sources. The output of each H-bridge is shown in figure 2. It can be noted that the switching frequency of the main H-bridge, which manages more than 80% of the total power, is the same frequency of the system, in this case, only 50 Hz. The frequency of the auxiliary H-Bridges is also low but increases as

the voltage level of the inverter become lower in the chain. Which means that the H-Bridge with DC link voltage (V) has switching frequency equal the switching frequency of the mulit-level inverter which is 5kHz. The voltage V that is used is 25 V and the maximum voltage generated from each leg is 325 V.

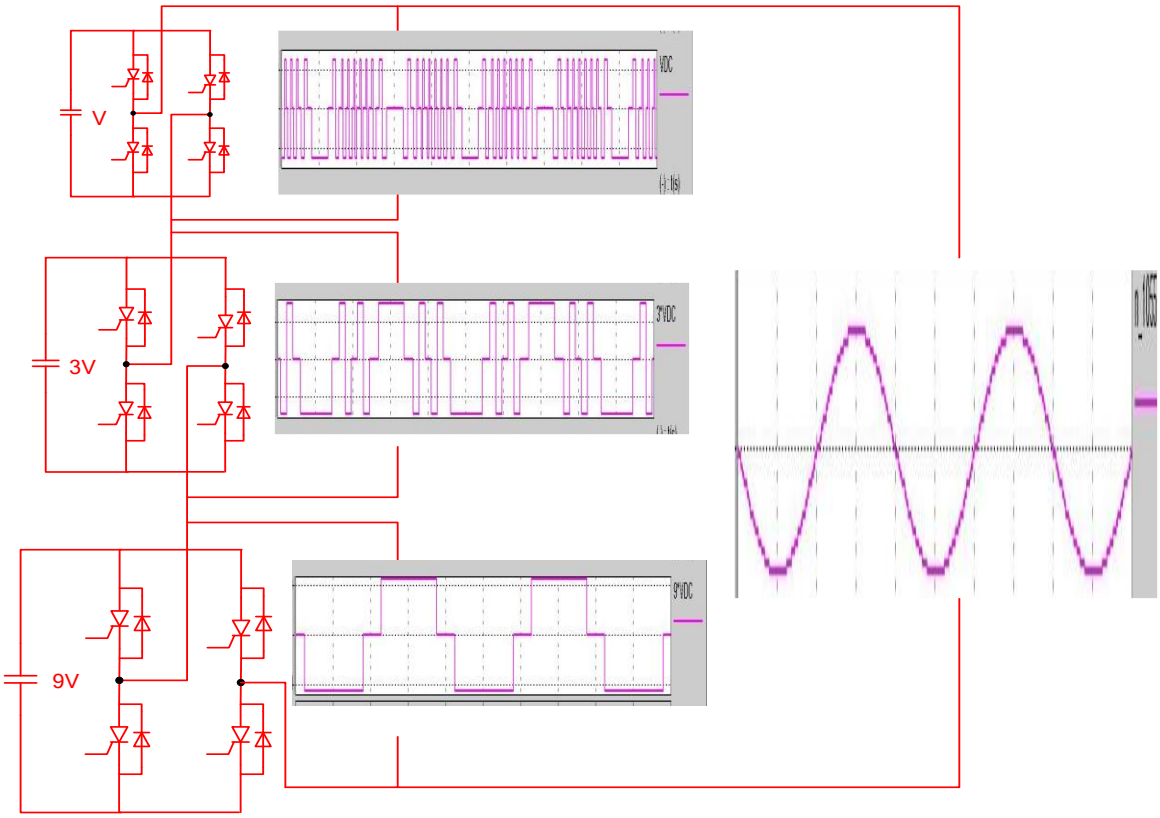

Figure 2. Asymmetric 27- level inverter waveforms

2.3 3D –SVPWM

The proposed 3D-SVPWM technique that is adopted in this work is presented in (Prats, Franquelo, Leon, Portillo, Galvan, & Carrasco, 2003). This technique is very simple and based on the geometrical consideration. Moreover, it is independent of the number of levels of the multi-level inverter. And more importantly, can be used under healthy condition and post an open circuit fault without modifications. The 3D space vector of the 27-level inverter is shown in figure 3.

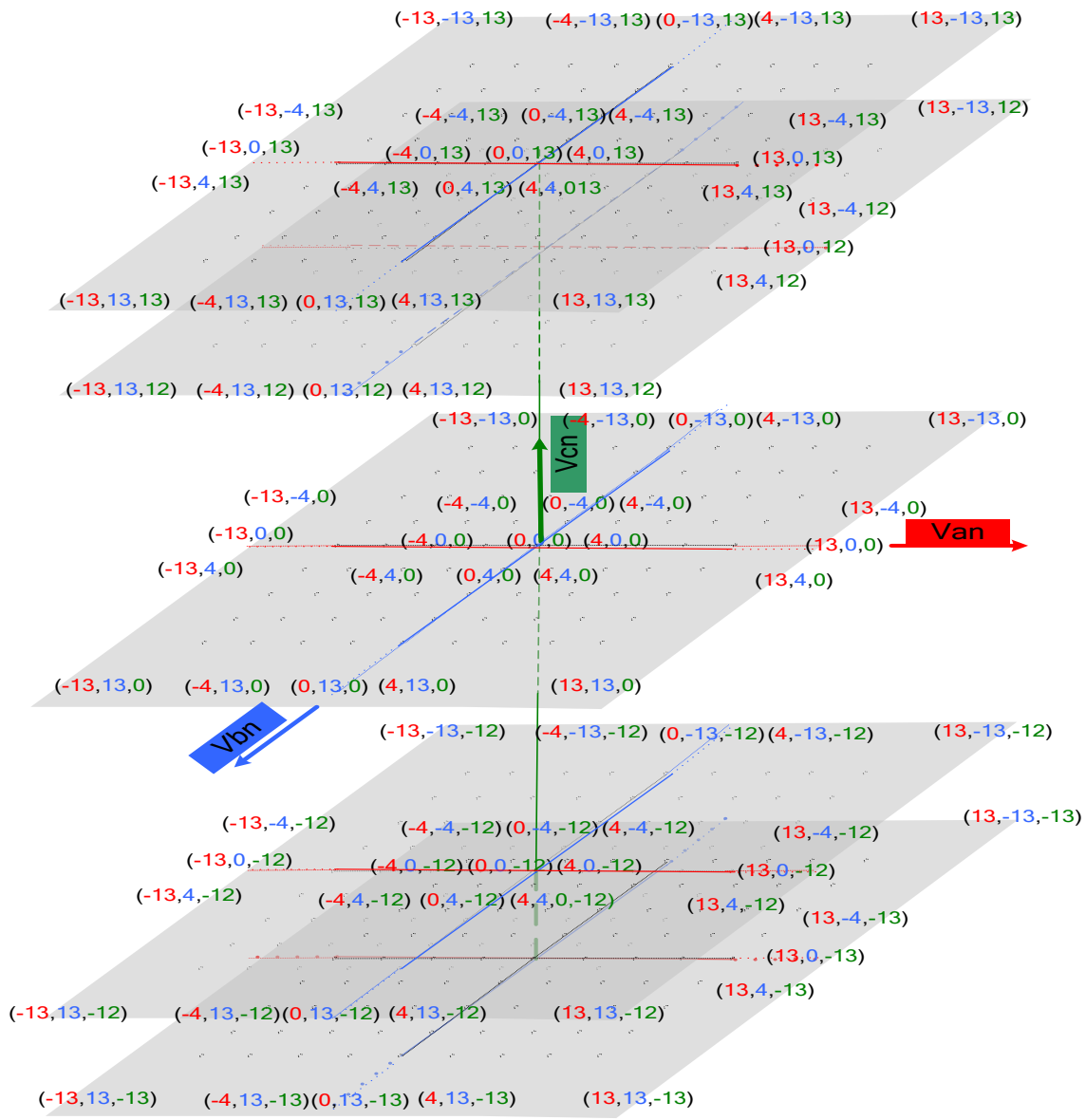

Figure 3. 27-level 3D SVM state diagram in abc coordinates.

The reference voltage will be pointing to sub-cube. This sub –cube can be identified using the components (a,b,c) which are the integer values of the reference voltage (V_ref) as shown in figure 4. This cube can be decomposed into six tetrahedrons. These tetrahedrons and the associated PWM waveforms are shown in Figure 5.

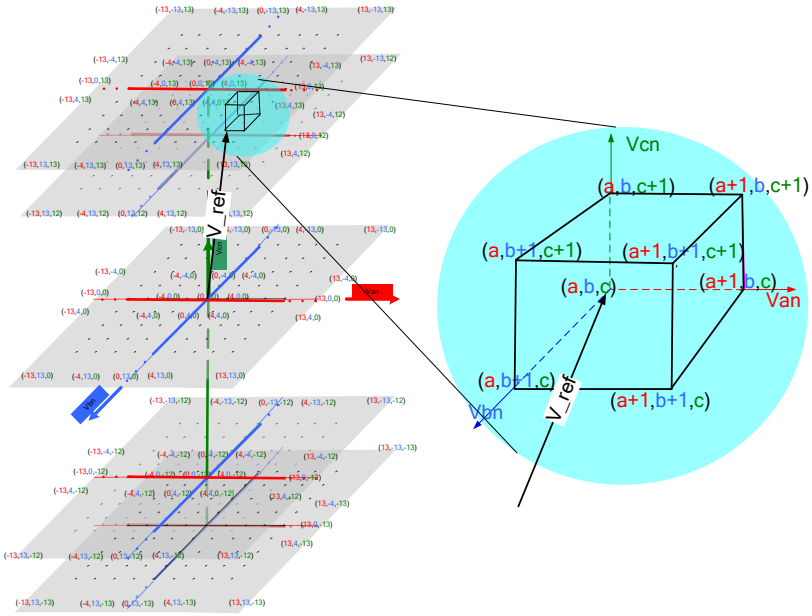

Figure 4. Origin of the Sub-cube where the reference voltage is found.

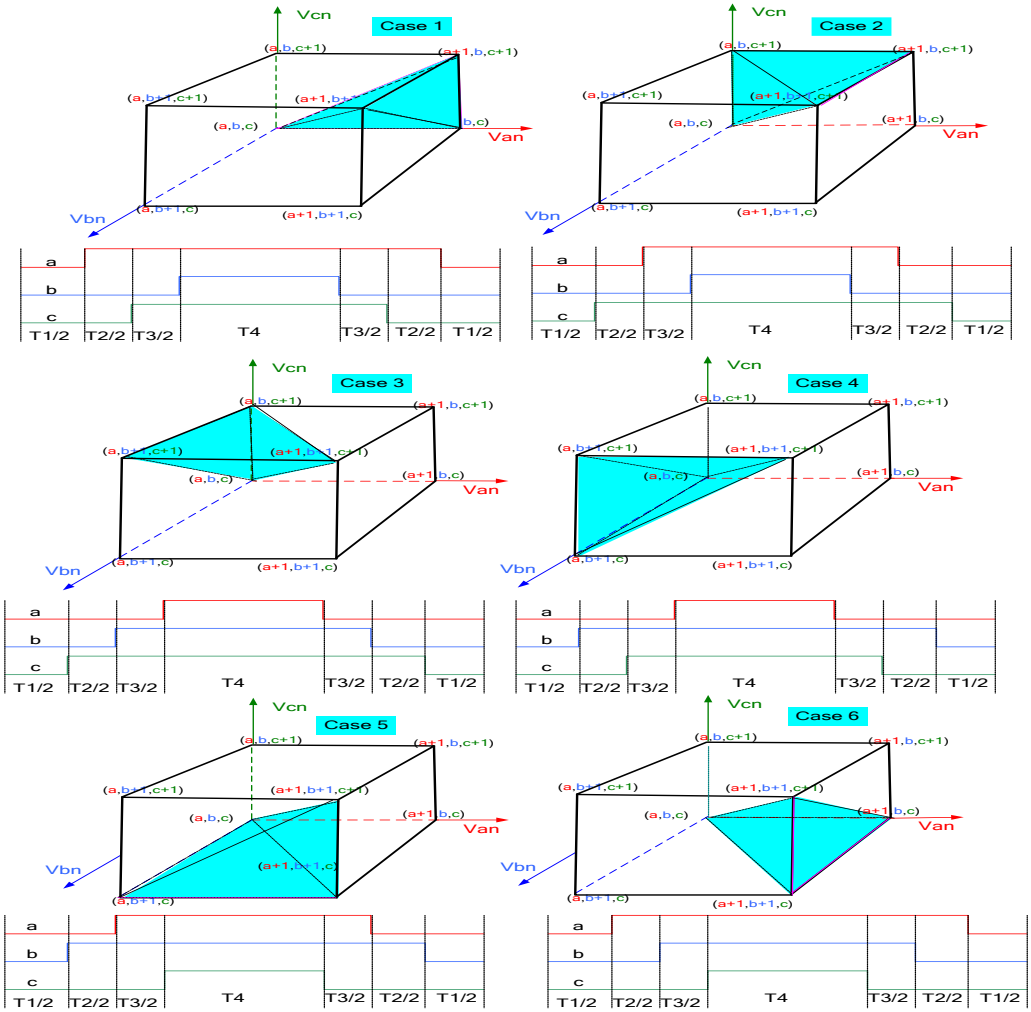

Figure 5 Switching sequence and timing diagram of type 3 used in SVPWM for the multi-level converter

The flow diagram of the 3D modulation algorithm for choosing the tetrahedron where the reference voltage is pointing to is shown in figure 6

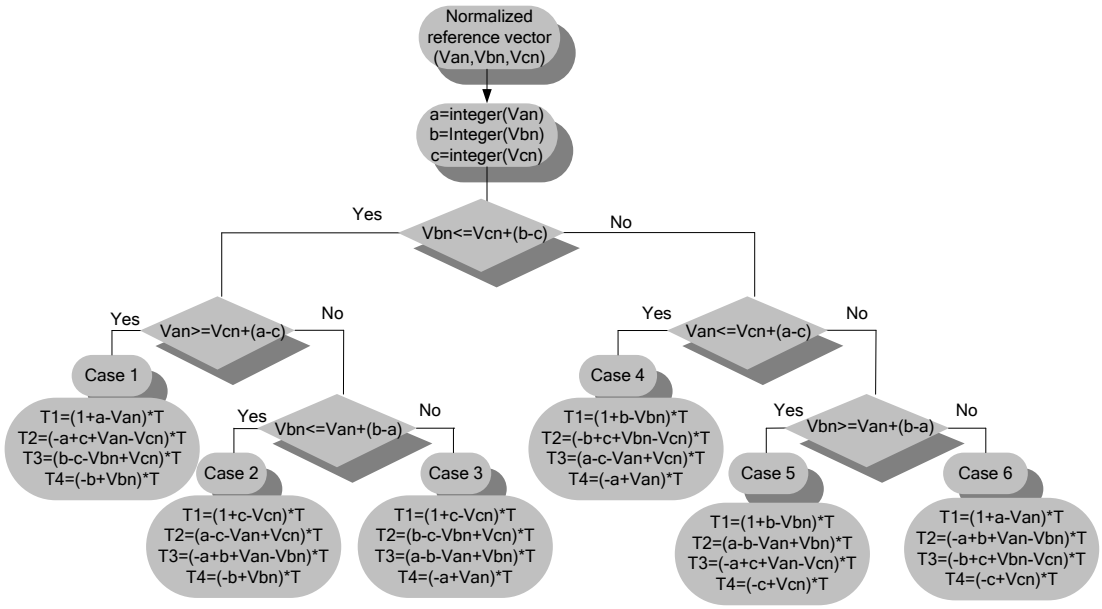

Figure 6 3-D algorithm for the selection of each tetrahedron with corresponding state vector

2.4 simulation results of a sensored speed control

Figure 7 shows the Indirect Rotor Field Orientation (IRFO) control structure proposed for the 27-level 4-leg PMSM drive. The reliability of this topology has been enhanced by adding the fourth leg to control the zero sequence component of the current in case of unhealthy operating condition in addition to the using the 3D SVPWM technique. The simulation of the PMSM drive system has been carried out using the SABER simulation package in sensored mode, pre, and post an open-circuit fault. The current controllers of the d-q components of the stator currents of the PMSM were designed such that the closed loop bandwidths were 300 Hz and damping ratios were 0.707, while the speed controller was designed such that the closed loop bandwidth was 10 Hz and damping ratio is 0.707. These designs specifications were chosen for the motor under healthy operating condition as well as under open-circuit fault condition. The PMSM motor parameters is given in

table 1.

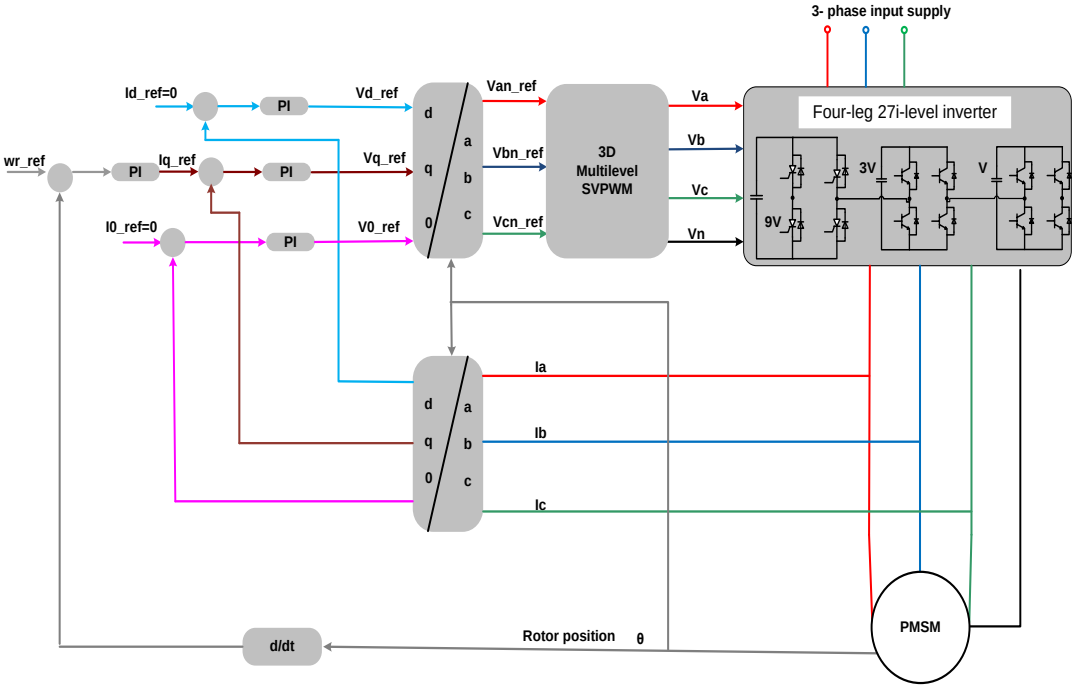

Figure 7 IRFO control topology for 27-level 4-leg PMSM drive.

Table 1. PMSM motor parameters

Rated speed	1500 rpm
Rated Torque	12 N.m
Rated Power	2.15 kW
kt	2N.m/A
ke	147V/Krpm
Inertia	20kg/cm2
R(ph-ph)	4Ω
L(ph-ph)	29.8 mH

The implementation of the above vector control structure in hardware is illustrated in the flow chart given in figure 8 This flow chart shows what is done in each PWM period starting from reading the Analog to Digital converters (ADCs) of the DSP to obtain both the stator currents and the stator dynamic current responses and ending of the

generating the PWM signals. The stability analysis of the IRFO control topology that is given in figure 7 is examined using root locus as shown in figure 9. The root locus of the closed loop system shows that the system is stable as the poles of the closed loop system exists in the left half of the root locus.

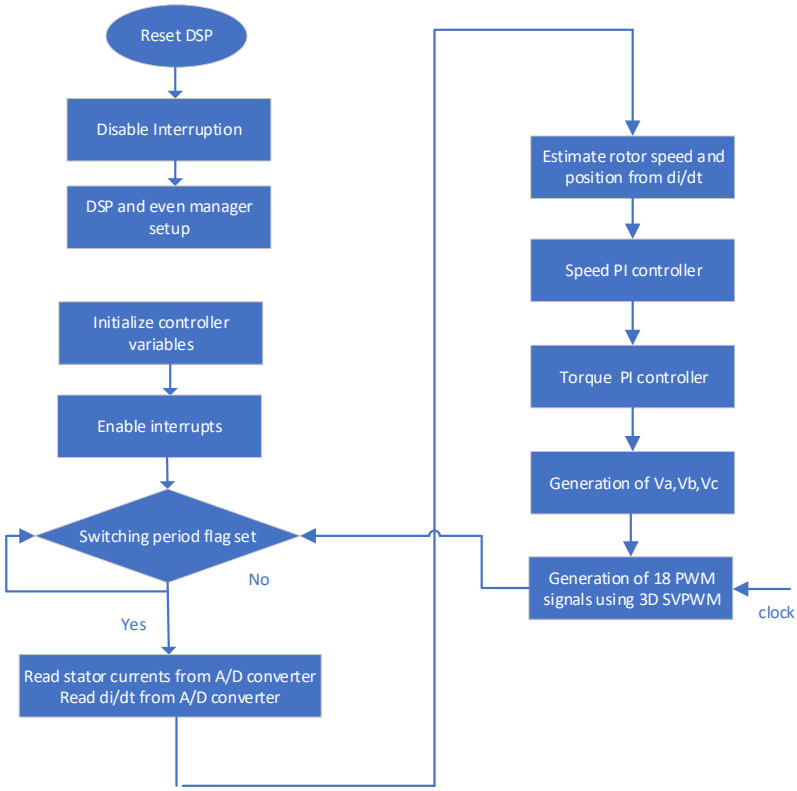

Figure 8. flow chart for the hardware implementation of the IRFO control topology

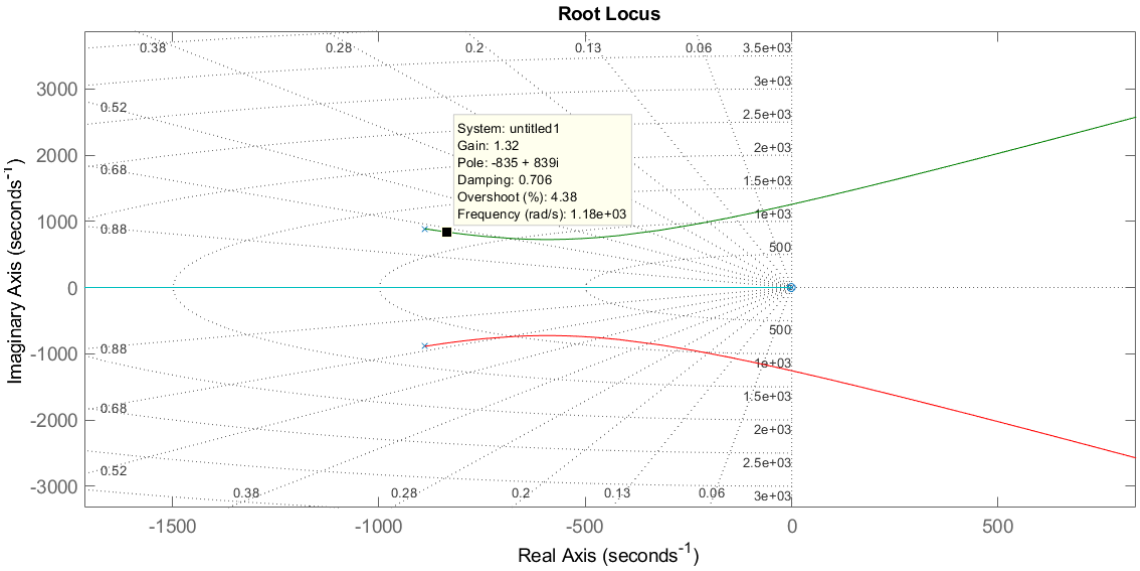

Figure 9. Root Locus for the IRFO control topology

The simulation results in figure 10 show the effectiveness of the PMSM drive system. The motor was running at speed equals to 1300 rpm at full load. In time intervals (2.5s-3s), (3.5s-4s), and (4s-4.5s) an open circuit fault was introduced to phase "a", phase "b" and phase "c" respectively. The controller could maintain the performance of the system post the open-circuit fault by increasing the remaining healthy currents by $\sqrt{3}$ as well as phase shifting them by 30 degrees away from the faulted phase. These actions are done automatically by the controller in this work without the need to do any extra actions as in (Saleh, & Sumner,2018). This is related to the using of 3D SVPWM in which the phase to neutral voltage in each leg can be generated separately unlike the using of 2D SVPWM.

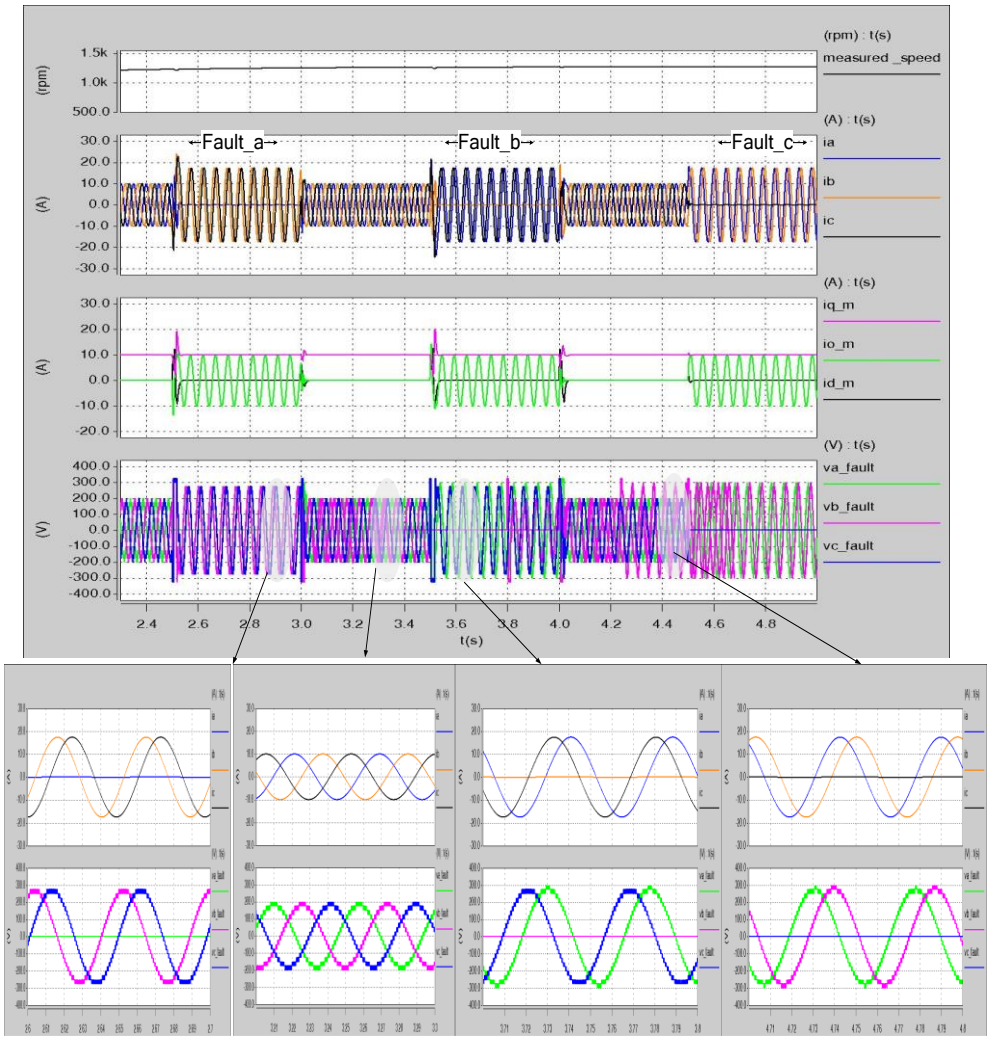

Figure10. Performance of a 4-phase multi-level inverter PMSM drive system under different operating conditions

3. Tracking the saturation saliency of PMSM

3.1 under healthy condition

In section 2.1, equation (3) has shown that the saturation saliency is inherently included in the model of the PMSM and reflected in the term (2θ) of both the self and mutual inductances. Based on that, the self and mutual inductances will vary according to the position of the rotor (θ). This variation will be reflected in the transient response of the three-line currents of the PMSM motor due to the switching actions. And so, the saturation saliency can be tracked by measuring these transient current responses during each PWM period. The algorithm to track the saturation saliency under health operating conditions is presented in this section. Figure 11 shows the case 3 switching sequence of the 4-leg 27-level inverter under healthy operating condition. The stator circuit when the vectors V0,V1, V2, and V3 are applied are shown in the same Figure.

Using the stator dynamic circuits shown in Figure 11 , the following equations hold true.

$$\begin{bmatrix} 0 \\ 0 \\ V_{DC} \end{bmatrix} = r_s * \begin{bmatrix} {i_a}^{(V1)} - {i_a}^{(V0)} \\ {i_b}^{(V1)} - {i_b}^{(V0)} \\ {i_c}^{(V1)} - {i_c}^{(V0)} \end{bmatrix} + \frac{d}{dt} \begin{bmatrix} l_{\sigma a} * ({i_a}^{(V1)} - {i_a}^{(V0)}) \\ l_{\sigma b} * ({i_b}^{(V1)} - {i_b}^{(V0)}) \\ l_{\sigma c} * ({i_c}^{(V1)} - {i_c}^{(V0)}) \end{bmatrix} + \begin{bmatrix} {e_a}^{(V1)} - {e_a}^{(V0)} \\ {e_b}^{(V1)} - {e_b}^{(V0)} \\ {e_c}^{(V1)} - {e_c}^{(V0)} \end{bmatrix} \quad (6)$$

$$\begin{bmatrix} 0 \\ V_{DC} \\ 0 \end{bmatrix} = r_s * \begin{bmatrix} {i_a}^{(V2)} - {i_a}^{(V1)} \\ {i_b}^{(V2)} - {i_b}^{(V1)} \\ {i_c}^{(V2)} - {i_c}^{(V1)} \end{bmatrix} + \frac{d}{dt} \begin{bmatrix} l_{\sigma a} * ({i_a}^{(V2)} - {i_a}^{(V1)}) \\ l_{\sigma b} * ({i_b}^{(V2)} - {i_b}^{(V1)}) \\ l_{\sigma c} * ({i_c}^{(V2)} - {i_c}^{(V1)}) \end{bmatrix} + \begin{bmatrix} {e_a}^{(V2)} - {e_a}^{(V1)} \\ {e_b}^{(V2)} - {e_b}^{(V1)} \\ {e_c}^{(V2)} - {e_c}^{(V1)} \end{bmatrix} \quad (7)$$

$$\begin{bmatrix} V_{DC} \\ 0 \\ 0 \end{bmatrix} = r_s * \begin{bmatrix} {i_a}^{(V3)} - {i_a}^{(V2)} \\ {i_b}^{(V3)} - {i_b}^{(V2)} \\ {i_c}^{(V3)} - {i_c}^{(V2)} \end{bmatrix} + \frac{d}{dt} \begin{bmatrix} l_{\sigma a} * ({i_a}^{(V3)} - {i_a}^{(V2)}) \\ l_{\sigma b} * ({i_b}^{(V3)} - {i_b}^{(V2)}) \\ l_{\sigma c} * ({i_c}^{(V3)} - {i_c}^{(V2)}) \end{bmatrix} + \begin{bmatrix} {e_a}^{(V3)} - {e_a}^{(V2)} \\ {e_b}^{(V3)} - {e_b}^{(V2)} \\ {e_c}^{(V3)} - {e_c}^{(V2)} \end{bmatrix} \quad (8)$$

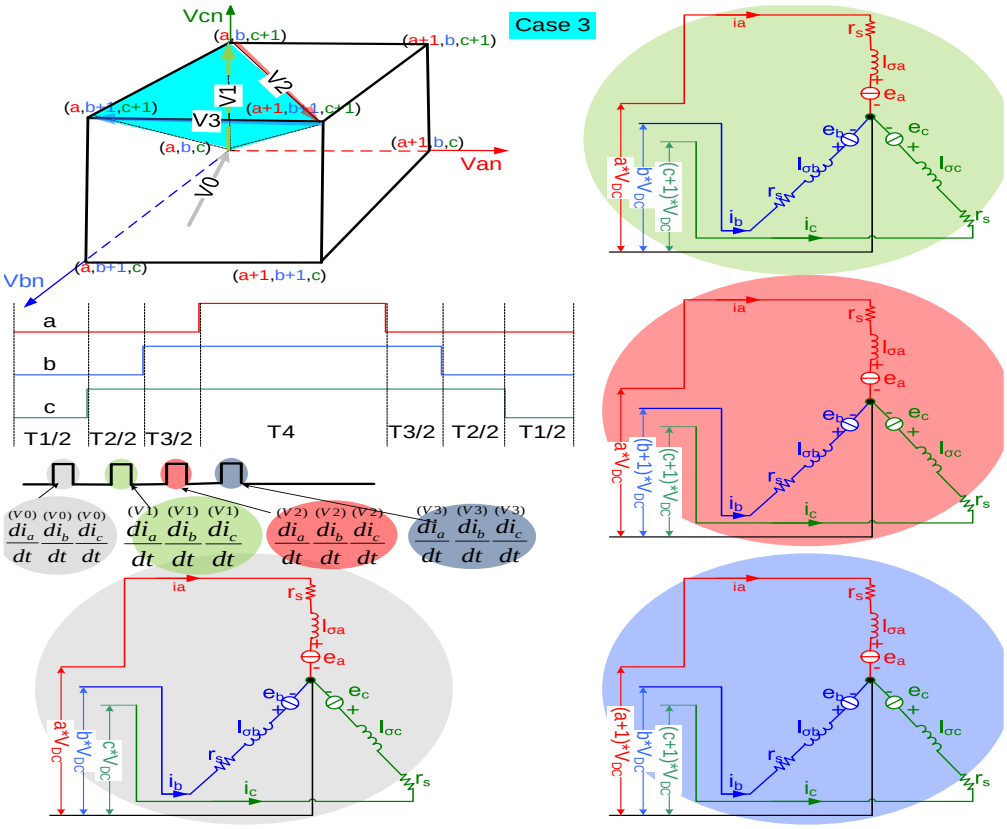

Figure11. Switching sequence for case 3 in 3D 27-level space diagram and the stator dynamic circuits under applying the voltage vectors V0, V1,V2 and V3 under healthy operating condition.

Assuming that the voltage drop across the stator resistances are small and the back emf can be neglected providing the time separation between the vectors is small, the following equations can be obtained using vector V0, V1,V2 and V3:-

$$\begin{bmatrix} 0 \\ 0 \\ V_{DC} \end{bmatrix} = \frac{d}{dt} \begin{bmatrix} l_{\sigma a} * \left(i_a{}^{(V1)} - i_a{}^{(V0)}\right) \\ l_{\sigma b} * \left(i_b{}^{(V1)} - i_b{}^{(V0)}\right) \\ l_{\sigma c} * \left(i_c{}^{(V1)} - i_c{}^{(V0)}\right) \end{bmatrix} \quad (9)$$

$$\begin{bmatrix} 0 \\ V_{DC} \\ 0 \end{bmatrix} = \frac{d}{dt} \begin{bmatrix} l_{\sigma a} * \left(i_a{}^{(V2)} - i_a{}^{(V1)}\right) \\ l_{\sigma b} * \left(i_b{}^{(V2)} - i_b{}^{(V1)}\right) \\ l_{\sigma c} * \left(i_c{}^{(V2)} - i_c{}^{(V1)}\right) \end{bmatrix} \quad (10)$$

$$\begin{bmatrix} V_{DC} \\ 0 \\ 0 \end{bmatrix} = \frac{d}{dt} \begin{bmatrix} l_{\sigma a} * \left(i_a{}^{(V3)} - i_a{}^{(V2)}\right) \\ l_{\sigma b} * \left(i_b{}^{(V3)} - i_b{}^{(V2)}\right) \\ l_{\sigma c} * \left(i_c{}^{(V3)} - i_c{}^{(V2)}\right) \end{bmatrix} \quad (11)$$

Finally the saliency position scalars P_a, P_b *and* P_c can be obtained as follows:-

$$\begin{bmatrix} P_a \\ P_b \\ P_c \end{bmatrix} = \frac{d}{dt} \begin{bmatrix} (i_a{}^{(V3)} - i_a{}^{(V2)}) \\ (i_b{}^{(V3)} - i_b{}^{(V2)}) \\ (i_c{}^{(V3)} - i_c{}^{(V2)}) \end{bmatrix} \quad (12)$$

By doing the same procedures for other cases, tables 1 can be constructed to track the saliency under healthy operating condition for four leg-multi-level inverter.

Table 2. Selection of pa, pb, and pc for a star-connected machine driven by 4-leg 27-level inverter under healthy operating condition

tetrahedron	Pa	Pb	Pc
Case1	$\frac{d}{dt}(i_a{}^{(V1)} - i_a{}^{(V0)})$	$\frac{d}{dt}(i_b{}^{(V3)} - i_b{}^{(V2)})$	$\frac{d}{dt}(i_c{}^{(V2)} - i_c{}^{(V1)})$
Case 2	$\frac{d}{dt}(i_a{}^{(V2)} - i_a{}^{(V1)})$	$\frac{d}{dt}(i_b{}^{(V3)} - i_b{}^{(V2)})$	$\frac{d}{dt}(i_c{}^{(V1)} - i_c{}^{(V0)})$
Case 3	$\frac{d}{dt}(i_a{}^{(V3)} - i_a{}^{(V2)})$	$\frac{d}{dt}(i_b{}^{(V2)} - i_b{}^{(V1)})$	$\frac{d}{dt}(i_c{}^{(V1)} - i_c{}^{(V0)})$
Case 4	$\frac{d}{dt}(i_a{}^{(V3)} - i_a{}^{(V2)})$	$\frac{d}{dt}(i_b{}^{(V1)} - i_b{}^{(V0)})$	$\frac{d}{dt}(i_c{}^{(V2)} - i_c{}^{(V1)})$
Case 5	$\frac{d}{dt}(i_a{}^{(V2)} - i_a{}^{(V1)})$	$\frac{d}{dt}(i_b{}^{(V1)} - i_b{}^{(V0)})$	$\frac{d}{dt}(i_c{}^{(V3)} - i_c{}^{(V2)})$
Case 6	$\frac{d}{dt}(i_a{}^{(V1)} - i_a{}^{(V0)})$	$\frac{d}{dt}(i_b{}^{(V2)} - i_b{}^{(V1)})$	$\frac{d}{dt}(i_c{}^{(V3)} - i_c{}^{(V2)})$

3.1 Post an open-circuit fault condition

the algorithm to track the saliency of the 4-leg inverter 27-level inverter under healthy operating condition as given in table 2 can't be applied in the cases of an open-circuit fault operating condition. This related to the fact that the dynamic current response of the faulted phase is equal zero and hence the position scalar related the faulted phase can't be constructed. To obtain the algorithm to track the saliency under an open-circuit operating condition the new stator dynamic circuits should be considered. Figure 12 shows the case 3 switching sequence of the 4-leg 27-level inverter under phase'b' open circuit fault operating conditions. The stator circuit when the vectors V0, V1, and V3 are applied are shown in same Figure 12 .

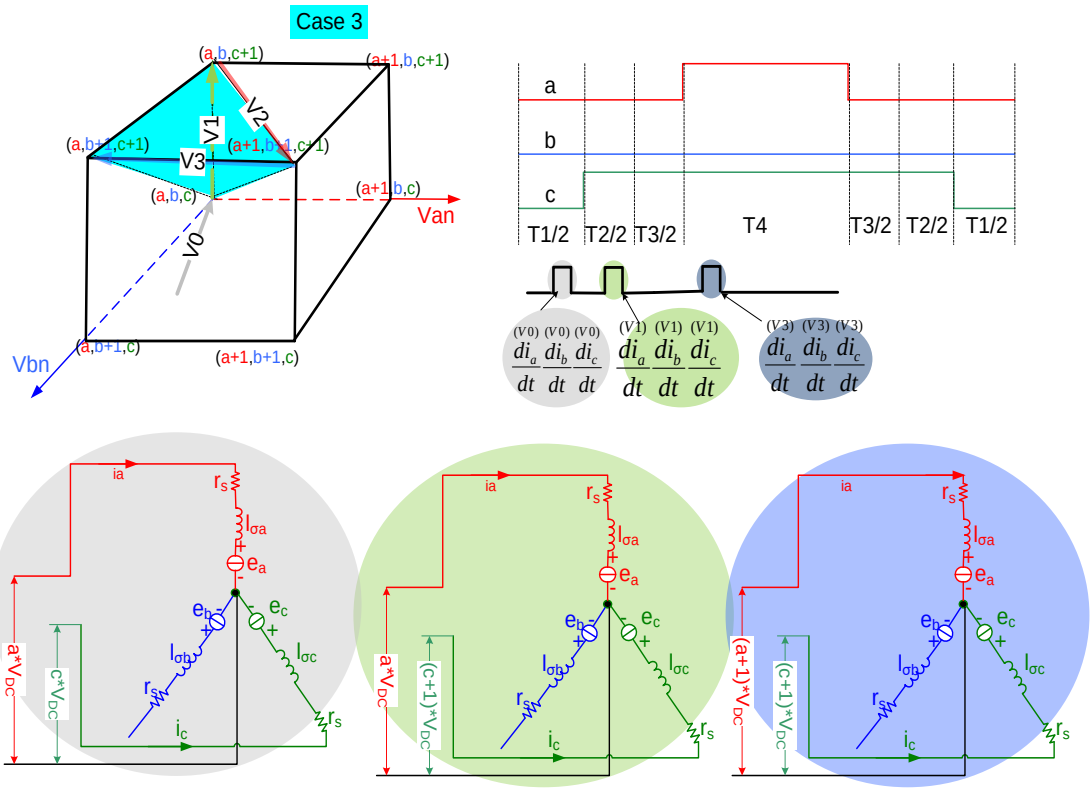

Figure12. Switching sequence for case 3 in 3D 27-level space diagram and the stator dynamic circuits under a applying the voltage vectors V0, V1,V2 and V3 in case of phase'b' open-circuit fault.

Using the stator dynamic circuits shown in Figure 10 , the following equations hold true.

$$\begin{bmatrix} 0 \\ V_{DC} \end{bmatrix} = r_s * \begin{bmatrix} i_a^{(V1)} - i_a^{(V0)} \\ i_c^{(V1)} - i_c^{(V0)} \end{bmatrix} + \frac{d}{dt}\begin{bmatrix} l_{\sigma a} * (i_a^{(V1)} - i_a^{(V0)}) \\ l_{\sigma c} * (i_c^{(V1)} - i_c^{(V0)}) \end{bmatrix} + \begin{bmatrix} e_a^{(V1)} - e_a^{(V0)} \\ e_c^{(V1)} - e_c^{(V0)} \end{bmatrix} \quad (13)$$

$$\begin{bmatrix} V_{DC} \\ 0 \end{bmatrix} = r_s * \begin{bmatrix} i_a^{(V3)} - i_a^{(V1)} \\ i_c^{(V3)} - i_c^{(V1)} \end{bmatrix} + \frac{d}{dt}\begin{bmatrix} l_{\sigma a} * (i_a^{(V3)} - i_a^{(V1)}) \\ l_{\sigma c} * (i_c^{(V3)} - i_c^{(V1)}) \end{bmatrix} + \begin{bmatrix} e_a^{(V3)} - e_a^{(V1)} \\ e_c^{(V3)} - e_c^{(V1)} \end{bmatrix} \quad (14)$$

By neglecting the voltage drop across stator resistance and the back emf, the following equations can be obtained using vector V0, V1 and V3:-

$$\begin{bmatrix} 0 \\ V_{DC} \end{bmatrix} = \frac{d}{dt}\begin{bmatrix} l_{\sigma a} * (i_a^{(V1)} - i_a^{(V0)}) \\ l_{\sigma c} * (i_c^{(V1)} - i_c^{(V0)}) \end{bmatrix} \quad (15)$$

$$\begin{bmatrix} V_{DC} \\ 0 \end{bmatrix} = \frac{d}{dt}\begin{bmatrix} l_{\sigma a} * (i_a^{(V3)} - i_a^{(V1)}) \\ l_{\sigma c} * (i_c^{(V3)} - i_c^{(V1)}) \end{bmatrix} \quad (16)$$

Finally the saliency position scalars P_a *and* P_c can be obtained as follows:-

$$\begin{bmatrix} P_a \\ P_c \end{bmatrix} = \frac{d}{dt}\begin{bmatrix} (i_a{}^{(V3)} - i_a{}^{(V2)}) \\ (i_c{}^{(V3)} - i_c{}^{(V2)}) \end{bmatrix} \quad (17)$$

P_b can deduced from P_a *and* P_c as follows:-

$$P_b = -(P_a + P_c) \quad (18)$$

By doing the same procedures for other cases and other phases, tables 3,4, and 5 can be constructed to track the saliency in case of open circuit fault.

Table 3. Selection of pa, pb, and pc for a star-connected machine driven by 4-leg 27-level inverter under phase'a' open-circuit fault.

tetrahedron	Pa	Pb	Pc
Case1	$-(P_b + P_c)$	$\frac{d}{dt}(i_b{}^{(V3)} - i_b{}^{(V2)})$	$\frac{d}{dt}(i_c{}^{(V2)} - i_c{}^{(V1)})$
Case 2	$-(P_b + P_c)$	$\frac{d}{dt}(i_b{}^{(V3)} - i_b{}^{(V2)})$	$\frac{d}{dt}(i_c{}^{(V1)} - i_c{}^{(V0)})$
Case 3	$-(P_b + P_c)$	$\frac{d}{dt}(i_b{}^{(V2)} - i_b{}^{(V1)})$	$\frac{d}{dt}(i_c{}^{(V1)} - i_c{}^{(V0)})$
Case 4	$-(P_b + P_c)$	$\frac{d}{dt}(i_b{}^{(V1)} - i_b{}^{(V0)})$	$\frac{d}{dt}(i_c{}^{(V2)} - i_c{}^{(V1)})$
Case 5	$-(P_b + P_c)$	$\frac{d}{dt}(i_b{}^{(V1)} - i_b{}^{(V0)})$	$\frac{d}{dt}(i_c{}^{(V3)} - i_c{}^{(V2)})$
Case 6	$-(P_b + P_c)$	$\frac{d}{dt}(i_b{}^{(V2)} - i_b{}^{(V1)})$	$\frac{d}{dt}(i_c{}^{(V3)} - i_c{}^{(V2)})$

Table 4. Selection of pa, pb, and pc for a star-connected machine driven by 4-leg 27-level inverter under phase'b' open-circuit fault.

tetrahedron	Pa	Pb	Pc
Case1	$\frac{d}{dt}(i_a{}^{(V1)} - i_a{}^{(V0)})$	$-(P_a + P_c)$	$\frac{d}{dt}(i_c{}^{(V2)} - i_c{}^{(V1)})$
Case 2	$\frac{d}{dt}(i_a{}^{(V2)} - i_a{}^{(V1)})$	$-(P_a + P_c)$	$\frac{d}{dt}(i_c{}^{(V1)} - i_c{}^{(V0)})$
Case 3	$\frac{d}{dt}(i_a{}^{(V3)} - i_a{}^{(V2)})$	$-(P_a + P_c)$	$\frac{d}{dt}(i_c{}^{(V1)} - i_c{}^{(V0)})$
Case 4	$\frac{d}{dt}(i_a{}^{(V3)} - i_a{}^{(V2)})$	$-(P_a + P_c)$	$\frac{d}{dt}(i_c{}^{(V2)} - i_c{}^{(V1)})$
Case 5	$\frac{d}{dt}(i_a{}^{(V2)} - i_a{}^{(V1)})$	$-(P_a + P_c)$	$\frac{d}{dt}(i_c{}^{(V3)} - i_c{}^{(V2)})$
Case 6	$\frac{d}{dt}(i_a{}^{(V1)} - i_a{}^{(V0)})$	$-(P_a + P_c)$	$\frac{d}{dt}(i_c{}^{(V3)} - i_c{}^{(V2)})$

Table 5. Selection of pa, pb, and pc for a star-connected machine driven by 4-leg 27-level inverter under phase'c' open-circuit fault.

tetrahedron	Pa	Pb	Pc
Case1	$\frac{d}{dt}(i_a{}^{(V1)} - i_a{}^{(V0)})$	$\frac{d}{dt}(i_b{}^{(V3)} - i_b{}^{(V2)})$	$-(P_a + P_b)$
Case 2	$\frac{d}{dt}(i_a{}^{(V2)} - i_a{}^{(V1)})$	$\frac{d}{dt}(i_b{}^{(V3)} - i_b{}^{(V2)})$	$-(P_a + P_b)$
Case 3	$\frac{d}{dt}(i_a{}^{(V3)} - i_a{}^{(V2)})$	$\frac{d}{dt}(i_b{}^{(V2)} - i_b{}^{(V1)})$	$-(P_a + P_b)$
Case 4	$\frac{d}{dt}(i_a{}^{(V3)} - i_a{}^{(V2)})$	$\frac{d}{dt}(i_b{}^{(V1)} - i_b{}^{(V0)})$	$-(P_a + P_b)$
Case 5	$\frac{d}{dt}(i_a{}^{(V2)} - i_a{}^{(V1)})$	$\frac{d}{dt}(i_b{}^{(V1)} - i_b{}^{(V0)})$	$-(P_a + P_b)$
Case 6	$\frac{d}{dt}(i_a{}^{(V1)} - i_a{}^{(V0)})$	$\frac{d}{dt}(i_b{}^{(V2)} - i_b{}^{(V1)})$	$-(P_a + P_b)$

Figure 13 shows the results of the simulation to tracking saliency under healthy operating condition as given in table 2 and under single-phase open-circuit fault as given in tables 3, 4, and 5. The motor was running at 500 rpm at full load and under healthy operating condition. Open-circuit faults in phases 'a' , 'b' and 'c' were introduced at time intervals (2-2.5), (3-3.5) and (4-4.5) respectively. Figure 13 shows that the new algorithm can track the saliency in the case of an open-circuit fault with the same quality as in healthy conditions.

4. Fully sensorless speed control of 4-leg multilevel inverter under unhealthy condition

The sensorless speed control for a PMSM motor driven by 4-leg 27-level inverter in healthy mode and post an open circuit fault has been implemented in simulation in the SABER modelling environment. The estimated position signals Pαβ are used as the input to a mechanical observer (Lorenz, Van Patten, 1991) to obtain the speed ω^ and a cleaned position θ^. Note that the simulation includes a minimum pulse width of 10 μs when di/dt measurements are made, similar to the experimental results of (Saleh, Asher, Sumner, Tomasini, & Qiang, 2009). This estimated speed ω^ and position θ^ are used to obtain a

fully sensorless speed control as shown in Figure 14.

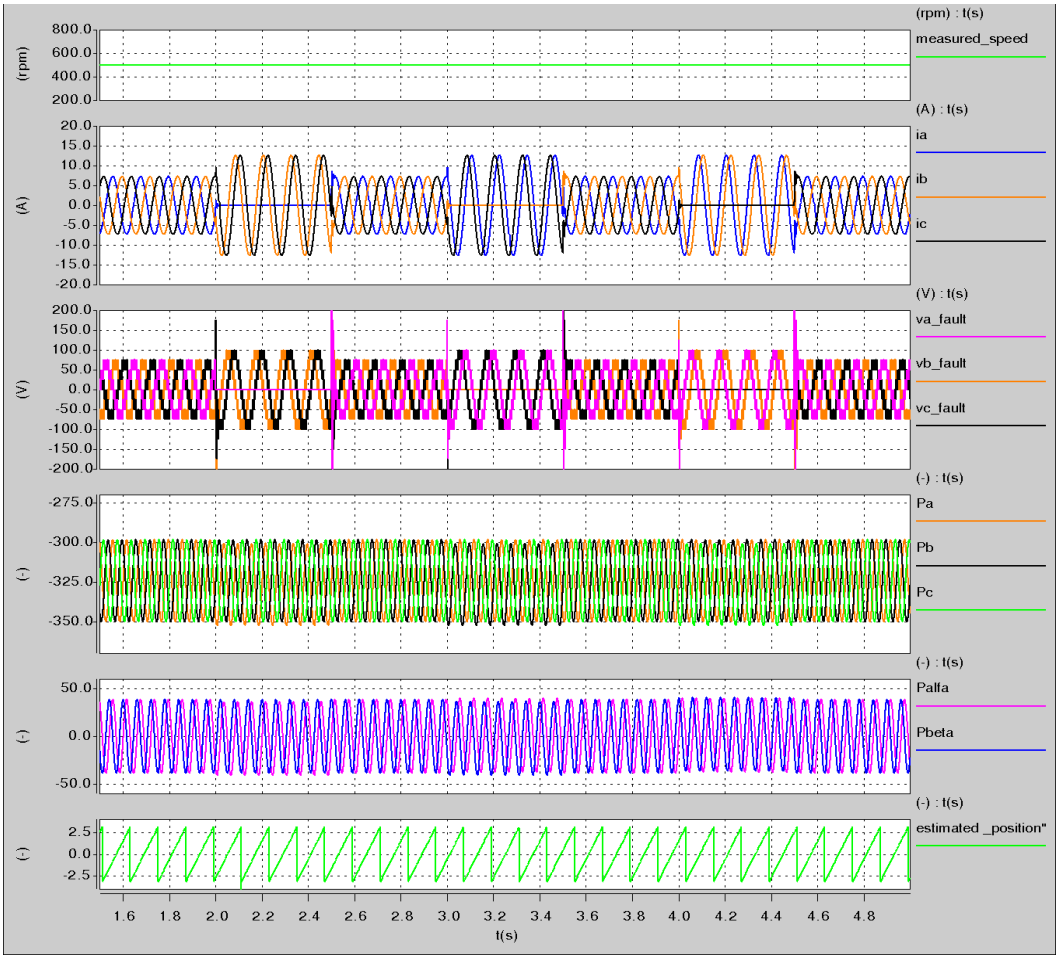

Figure 13 track the saliency in a 4-leg 27-level inverter using 3D SVPWM under healthy operating condition and post an open-circuit fault.

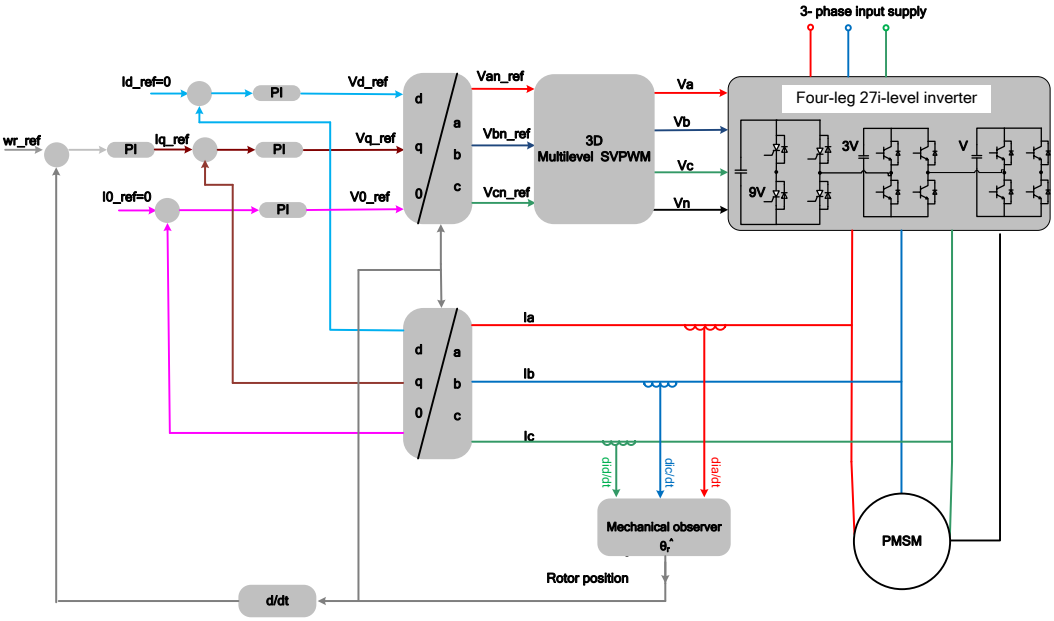

Figure 14. The sensorless vector control structure for the 4-leg 27-level inverter PMSM drive under a open-circuit fault.

Figure 15 shows the results of sensorless low-speed control of a PMSM motor using the algorithm proposed in this paper. The motor was running in healthy mode at a speed of 30 rpm. At t=2 s an open circuit fault is introduced to phase ‘a’. Then at t=2.5 s a speed step command from 30 rpm to zero was applied to the motor. Between t=3s and t=4s, the fault in phase ‘a’ is removed and the motor return to run in healthy mode. At t=4s, an open circuit was introduced to phase’b’. after that, at t= 4.5 s, a speed steps command from zero to -30 rpm was applied to the motor. Between time t=5s and t=6s, the fault is removed from phase’b’ and the motor returned to run in a healthy operating condition. Finally, at time t=6s, an open circuit was introduced to phase’c’. Figure 15 shows that the motor responded to the speed step with a good transient and steady-state response even the motor was running under an open circuit fault.

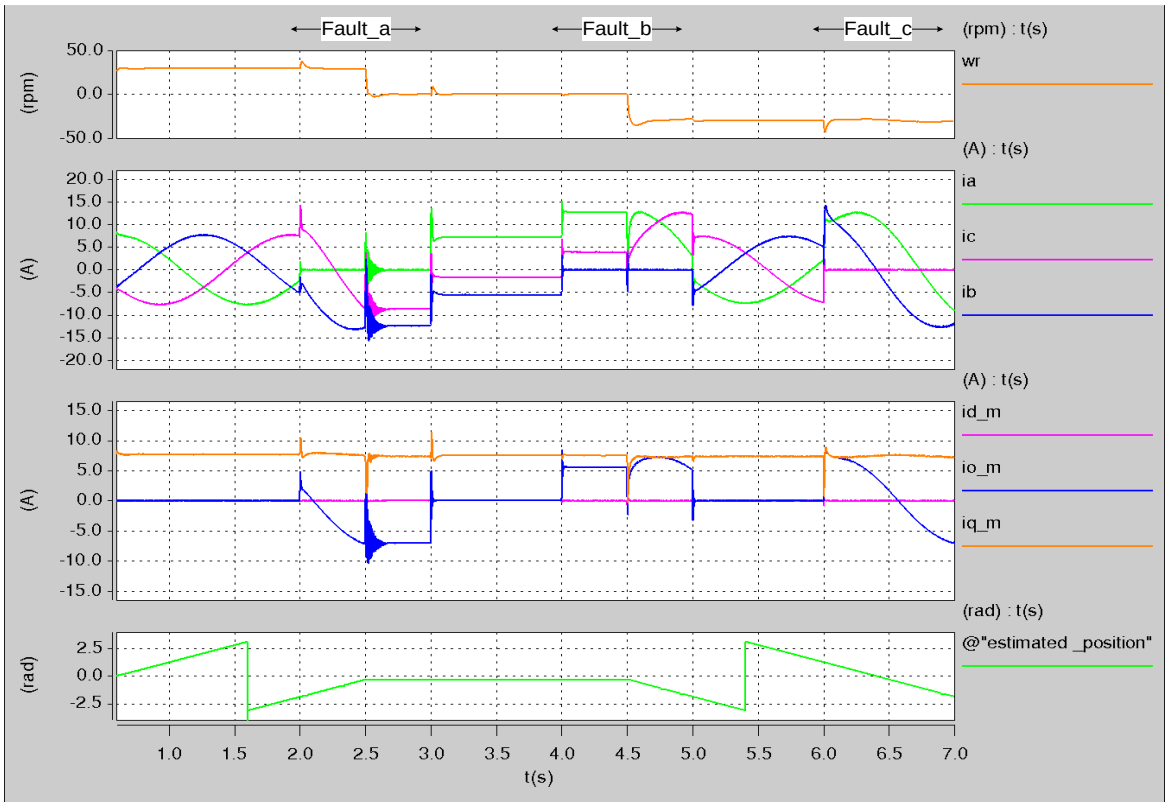

Figure 15. Fully sensorless speed steps between 30 rpm, 0 to 30 rpm under healthy condition and under open circuit fault condition.

Figure 16 shows results similar to the results shown in Figure 15 but with higher speed steps commanded from the system. The figure shows the effectiveness of the system in responding to the high-speed steps (from 500 rpm to -500 rpm back to 500 rpm) in the healthy case as well as the case of an open circuit.

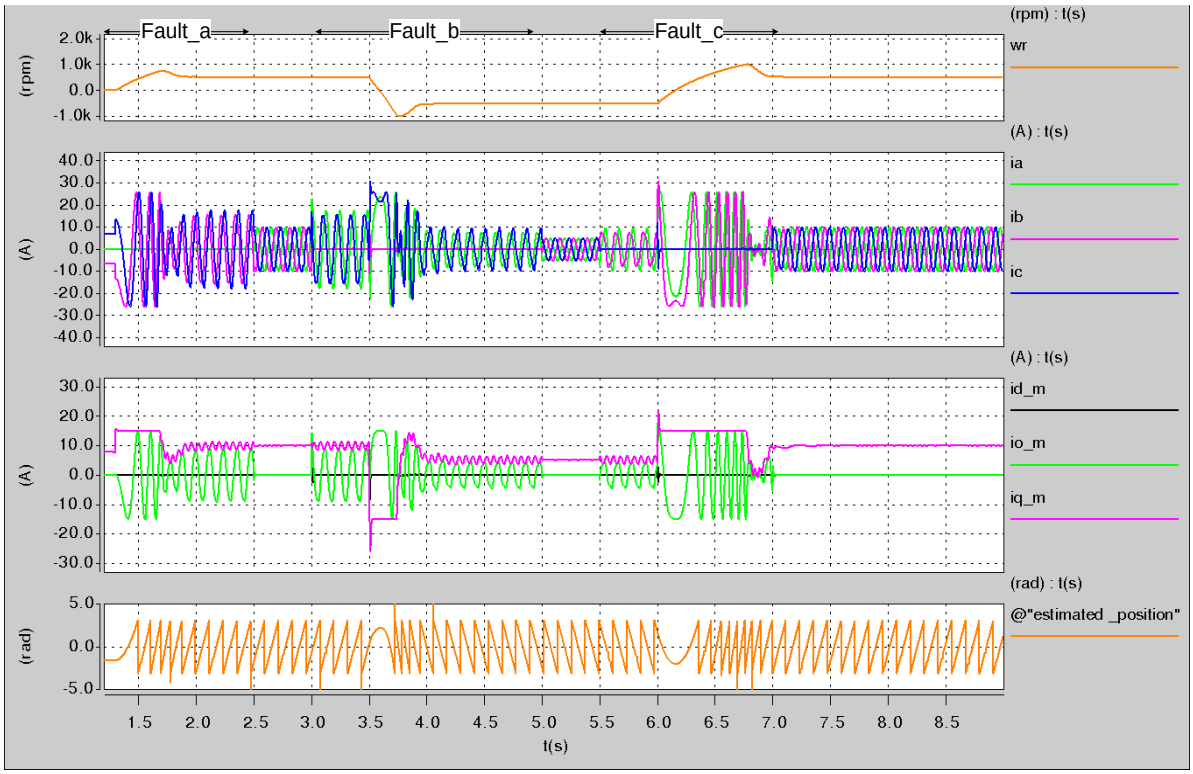

Figure 16. Fully sensorless speed steps between 500 rpm and -500 rpm under healthy condition and under open circuit fault condition.

Figure 17 demonstrates the stability of the fully sensorless system when a load disturbance is applied at low speed (200 rpm) in both healthy modes and under open phase fault conditions. The results show that the system maintains the speed in all the cases.

5. Conclusion

This paper has presented a novel technique to track the saturation saliency of a PMSM fed by a 4-leg 27-level inverter in the case of a single-phase open-circuit fault. The new technique is based on measuring the transient current response of the motor line currents due to the 27-level inverter switching actions. The proposed method can track the saliency

of the motor under healthy conditions post an open-circuit fault condition. The new technique is applicable to track the rotor slotting saliency in IMs (14*fr). The results have shown the effectiveness of the new technique in increasing the safety measures in critical systems that need continuous operation. In future, the research will continue in the fields of sensor less control of PMSM under other types of faults such as short-circuit. In addition, other techniques to obtain a fault-tolerant will be investigated to obtain a sensorless control

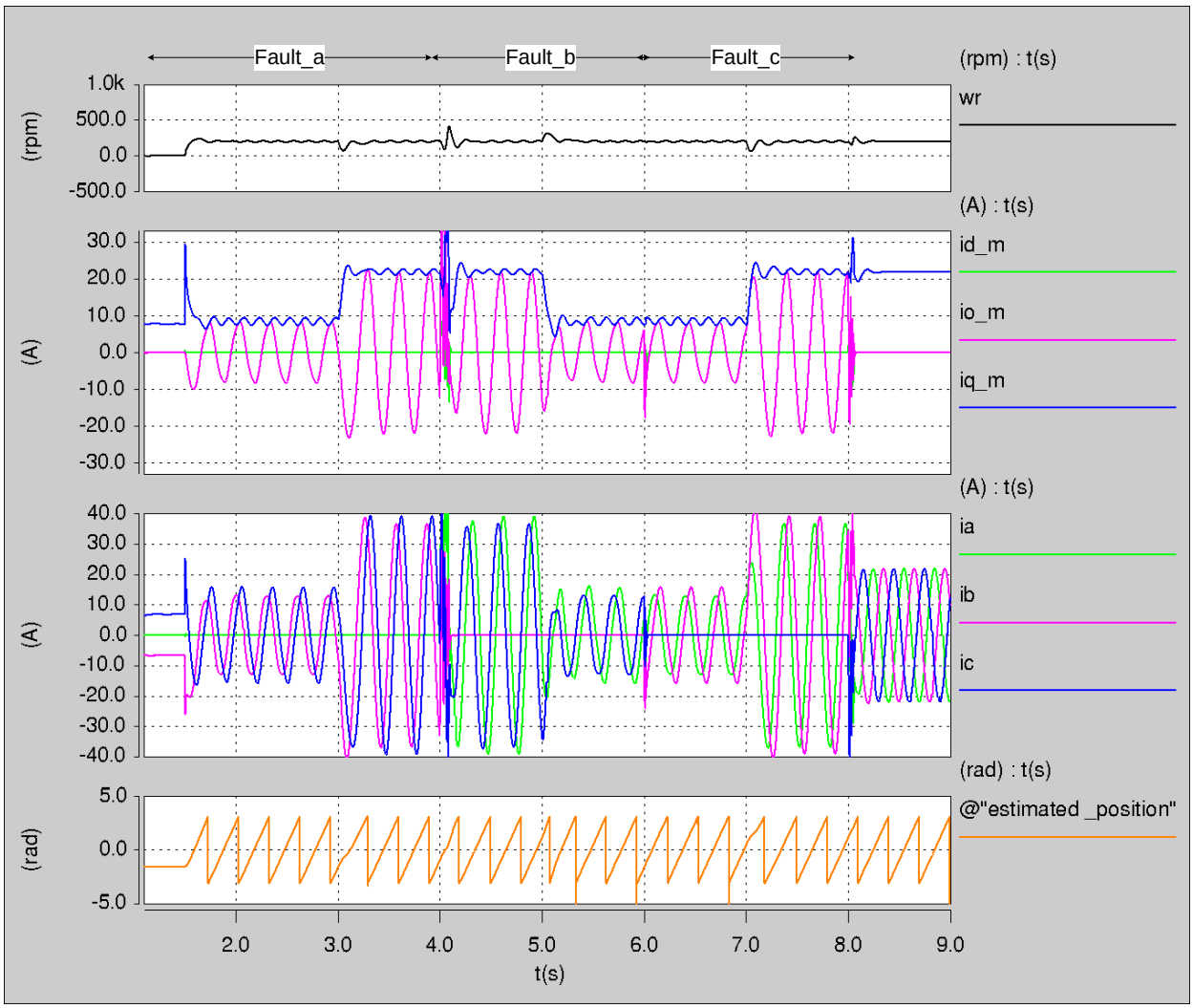

Figure 17. Fully sensorless full load steps under healthy condition and under open circuit fault condition

References

Ying, J., & Gan, H. (2012, June). High power conversion technologies and trend. in Proc. Proceedings of The 7th International Power Electronics and Motion Control Conference (pp. 1766-1770), Harbin, China.

Marzoughi, A., Burgos, R., Boroyevich, D., & Xue, Y. (2014, November). Investigation and comparison of cascaded H-bridge and modular multilevel converter topologies for medium-voltage drive application. In IECON-40th Annual Conference of the IEEE Industrial Electronics Society (pp. 1562-1568). Dallas, TX.

Qashqai,P., Sheikholeslami, A., Vahedi, H., & Al-Haddad, K.(2015,October). A Review on Multilevel Converter Topologies for Electric Transportation Applications. In 2015 IEEE Vehicle Power and Propulsion Conference (VPPC)(pp. 1-6), Montreal, QC.

Yu,Y., Konstantinou, G., Hredzak,B. & Agelidis,V.G. (2016). Power Balance of Cascaded H-Bridge Multilevel Converters for Large-Scale Photovoltaic Integration. IEEE Trans. Power Electron. 31, 1, pp.292 – 33.

Bhagwat, P.M., & Stefanovic,V.R. (1983). Generalized structure of a multilevel PWM inverter. IEEE Trans. Ind. Appl. 19,1057-1069.

Lai,S.J., & Peng, Z.F.(1996). Multi-level converters-A new breed of power converters. IEEE Trans. Ind. Appl.32,509-517.

Okazaki,Y., Matsui, H., Moses,M., Muhoro,M., Hagiwara ,M., & Akagi, H.(2016). Capacitor-Voltage Balancing for a Modular Multilevel DSCC Inverter Driving a Medium-Voltage Synchronous Motor. IEEE Trans. On Industry Applications, 52, 5, 4074-4083,2016.

Nabae, A., Takahashi,I., & Akagi,H. (1981). A new neutral-point clamped PWM inverter. IEEE Trans. Ind. Applicat.17, 5,518-523.

P. Hammond, P. (1997). A new approach to enhance power quality for medium voltage ac drives. IEEE Trans. Ind. Applicat., 33, 1, 202-208.

Meynard,A.T., Foch,H., Thomas, P., Courault, J., Jakob,R .& Nahrstaedt,M.(2002). Multicell converter: Basic concepts and industry applications," IEEE Trans. Ind. Electron. 49, 5, 955-964

Adiuku, O.C, Beig, R.A, & Kanukollu, S.(2015,February). Sensorless Closed Loop V/f Control of Medium-Voltage High-Power Induction Motor with Synchronized

Space Vector PWM. In 2015 IEEE 8th GCC Conference & Exhibition (pp. 1-6), Muscat. Oman

Wang, S. & Lu,Z. (2010, February). Study on Wide Range Robust Speed Sensorless Control of Medium Voltage Induction Motor. In Twenty-Fifth Annual IEEE Applied Power Electronics Conference and Exposition (APEC) (pp. 1542-1546). Palm Springs, CA

Kim,I. Chan,R., & Kwak,S. (2017). Model predictive control method for CHB multi-level inverter with reduced calculation complexity and fast dynamics. IET Electric Power Applications. 11, 5,784-792.

Kant, P., & Singh,B. (2018,December). Sensorless Vector Controlled Induction Motor Drive for Medium Power Applications. In IEEE International Conference on Power Electronics, Drives and Energy Systems (PEDES)(pp. 1-5), Chennai, India.

Scelba,G., Scarcella,G., Foti,S., De Caro, S., & Testa, A. (2017, September). Self-sensing control of open-end winding PMSMs fed by an asymmetrical hybrid multilevel inverter. In IEEE International Symposium on Sensorless Control for Electrical Drives (SLED)(pp. 165-172). Catania, Itlay.

Saleh,K., Asher,G., Sumner, M., Tomasini, M., & Qiang. G.(2009, September). Low Speed Sensorless Control of an Induction Motor Fed by Multilevel Converter to Reduce Current Distortion. In 13th European Conference on Power Electronics and Applications (EPE) (pp. 1-10), Barcelona, Spain.

Saleh,K. , Sumner, M.(2016). Modelling and Simulation of a Sensorless Control of a True Asymmetric Cascade H-Bridge Multilevel Inverter PMSM Drives. International Journal of Power Electronics and Drive System (IJPEDS). 7,2, 397~415

Welchko, A.B., Lipo, A.T., Jahns, M.T. & Schulz, S.E.(2004). Fault tolerant three-phase AC motor drive topologies: a comparison of features, cost, and limitations. IEEE Trans. Power Electron., 19, 4, 1108 – 1116.

Haimin, T., Duarte, L.J., & Hendrix, M.A. (2008) .Line-interactive UPS using a fuel cell as the primary source. IEEE Trans. Ind. Electron.,55, 8, 3012 -3021

Zhang, W., Xu, D., Enjeti, N.P., Li,H., Hawke, T.J.,& Krishnamoorthy,S.H. (2014). Survey on Fault-Tolerant Techniques for Power Electronic Converters. IEEE Transactions on Power Electronics, v29, 12,6319-6331..

Lezana, P., Pou, J. Meynard, T.A., Rodriguez, J., Ceballos, S., & Richardeau, F. (2010). Survey on Fault Operation on Multilevel Inverters. , IEEE Transactions on Industrial Electronics, 57, 7,2207-2218.

Campos-Delgado, D. U., Espinoza-Trejo, D. R., & Palacios, E. (2008). Fault tolerant control in variable speed drives: a survey. Electric Power Applications, IET , 2, 2, 121-134.

Rodriguez, M.A., Claudio, A., Theilliol, D., Vela, L.G., & Hernandez, L.(2008, November). A strategy to replace the damaged element for fault-tolerant induction motor drive. In Electrical Engineering, Computing Science and Automatic Control, CCE 2008. 5th International Conference (51-55), Mexico City, Mexico

Jen-Ren, F & Lipo, T.A. (1993, October). Disturbance free operation of a multiphase current regulated motor drive with an opened phase. In Industry Applications Society Annual Meeting, Conference Record of the 1993 IEEE (637-644). Toronto, Ontario, Canada, Canada

Mohammadpour, A., Sadeghi, S., & Parsa, L. (2014). A Generalized FaultTolerant Control Strategy for Five-Phase PM Motor Drives Cosidering Star, Pentagon, and Pentacle Connections of Stator Windings, IEEE Transactions on Industrial Electronics, , 61, 1, 63-75.

Yi, Z., Hongge,S. , & Bin, X. (2008, October). Optimization of neutral shift in cell-fault treatment for cascaded H-bridge inverter. 2008 International Conference on Electrical Machines and Systems (1683–1685), Wuhan, China

Lezana, P. & Ortiz, G. (2009). Extended operation of cascade multicell converters under fault condition. IEEE Trans. Ind. Electron., 56, 7,2697–2703.

Correa, P., Pacas, M., Rodriguez, J. (2006, July). Modulation Strategies for Fault Tolerant Operation of H-Bridge Multilevel Inverters. IEEE International Symposium on Industrial Electronics (1589-1594), Montreal, Que., Canada

Saleh, K. & Sumner, M. (2016). Modeling and simulation of sensorless control of four-leg inverter PMSM drives in the case of a single-phase open circuit fault. Turkish Journal of Electrical Engineering & Computer Sciences. 24. 3807-3820·

Saleh, K. & Sumner, M. (2018, June). Sensorless Control of a Fault Tolerant Multi-level Inverter PMSM Drives in Case of an Open Circuit Fault(883-888). In International Symposium on Power Electronics, Electrical Drives, Automation and Motion (SPEEDAM), Amalfi, Italy.

Prats, M.M., Franquelo, G.L., Leon, I.J,Portillo, R., Galvan, E. & Carrasco, M.J. (2003, November). A SVM-3D generalized algorithm for multilevel converters, In 29th Annual Conference of the IEEE Industrial Electronics Society IECON'03 (24-29), Roanoke, VA, USA.

Lorenz, D.R. , K.W. Van Patten, W.K. (1991) . High-Resolution Velocity Estimation for All-Digital, ac Servo Drives. IEEE transactions on industry applications, 27, 701 – 705.